Since January 2020 Elsevier has created a COVID-19 resource centre with free information in English and Mandarin on the novel coronavirus COVID-19. The COVID-19 resource centre is hosted on Elsevier Connect, the company's public news and information website.

Analytica Chimica Acta 1188 (2021) 339207

Contents lists available at ScienceDirect

Analytica Chimica Acta

journal homepage: www.elsevier.com/locate/aca

Label-free detection of SARS-CoV-2 Spike S1 antigen triggered by electroactive gold nanoparticles on antibody coated fluorine-doped tin oxide (FTO) electrode

Akanksha Roberts, Subhasis Mahari, Deepshikha Shahdeo, Sonu Gandhi*

DBT-National Institute of Animal Biotechnology (NIAB), Hyderabad, 500032, Telangana, India

HIGHLIGHTS

- Label-free electrochemical immunosensor fabricated with AuNPs for rapid detection of SARS-CoV-2 Spike S1.
- Developed immunosensor showed ultra-low detection of Spike S1 upto 120 fM in spiked saliva sample.
- The developed label free immunosensor showed high sensitivity, specificity, repeatability, and storage stability.

GRAPHICAL ABSTRACT

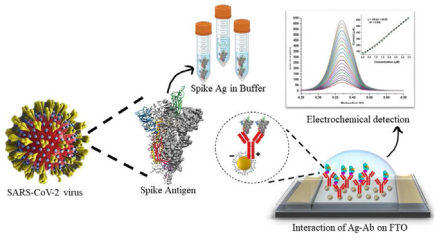

Electrochemical immunosensor modified with AuNPs/SARS-CoV-2Ab for detection of SARS-CoV-2 Spike S1 antigen.

ARTICLE INFO

Article history:
Received 2 September 2021
Received in revised form
4 October 2021
Accepted 19 October 2021
Available online 21 October 2021

Keywords:
SARS-CoV-2
Immunosensor
Gold nanoparticles
Spike antigen
Voltammetry

ABSTRACT

Severe acute respiratory syndrome coronavirus 2 (SARS-CoV-2, also known as 2019-nCov or COVID-19) outbreak has become a huge public health issue due to its rapid transmission making it a global pandemic. Here, we report fabricated fluorine doped tin oxide (FTO) electrodes/gold nanoparticles (AuNPs) complex coupled with in-house developed SARS-CoV-2 spike S1 antibody (SARS-CoV-2 Ab) to measure the response with Cyclic Voltammetry (CV) and Differential Pulse Voltammetry (DPV). The biophysical characterisation of FTO/AuNPs/SARS-CoV-2Ab was done via UV–Visible spectroscopy, Dynamic Light Scattering (DLS), and Fourier Transform Infrared Spectroscopy (FT-IR). The fabricated FTO/AuNPs/SARS-CoV-2Ab immunosensor was optimised for response time, antibody concentration, temperature, and pH. Under optimum conditions, the FTO/AuNPs/Ab based immunosensor displayed high sensitivity with limit of detection (LOD) up to 0.63 fM in standard buffer and 120 fM in spiked saliva samples for detection of SARS-CoV-2 spike S1 antigen (Ag) with negligible cross reactivity Middle East Respiratory Syndrome (MERS) spike protein. The proposed FTO/AuNPs/SARS-CoV-2Ab based biosensor proved to be stable for up to 4 weeks and can be used as an alternative non-invasive diagnostic tool for the rapid, specific and sensitive detection of SARS-CoV-2 Spike Ag traces in clinical samples.

* Corresponding author.
E-mail addresses: gandhi@niab.org.in, sonugandhi@gmail.com (S. Gandhi).

https://doi.org/10.1016/j.aca.2021.339207
0003-2670/

1. Introduction

SARS-CoV-2 is a single positive strand RNA virus consisting of four structural proteins including spike, envelope, matrix and nucleocapsid proteins and is responsible for respiratory tract illness [1]. In December 2019, an outbreak of pneumonia was observed in Wuhan, China and the causative pathogen was identified as a new type of coronavirus [2–6] and named as 2019 novel coronavirus (2019-nCoV) by the World Health Organization (WHO). For early diagnosis, chest computed tomography (CT) [7–10] was used whereas in the analytical stage, real-time reverse-transcriptase polymerase chain reaction (RT-PCR) [11–14] remains the standard reference test for the etiologic diagnosis of SARS-CoV-2 [15,16]. However, since both these conventional techniques are time consuming, laborious processes and may sometimes give false negative results due to low titre value, rapid mass screening is not possible which is the need of the hour to manage the spread of the virus, especially from non-symptomatic patients. In order to overcome the above disadvantages of conventional methods, various serological assay and biosensor [17] based detection methods have gained research interest which include Enzyme Linked Immunosorbent Assays (ELISA) [18], Lateral Flow Assays (LFA) [19], Field Effect Transistors (FET) [20], etc. Recently, integrated Internet of Things (IOT) and Clustered regularly interspaced short palindromic repeats (CRISPR) based techniques are being introduced as supplemental tools for rapid diagnosis [21–24]. However, this area still needs a lot of research as the sensors require higher sensitivity and specificity for the detection of SARS-CoV-2.

Biosensors are sensitive, specific, stable, easy to use, require less sample size, time, portable and most importantly can be customised to detect the target analyte of interest. Immunosensors can be used to detect toxins [25], narcotic drugs [26–29], viruses [30–32] by use of different bioreceptors such as deoxyribonucleic acid (DNA) [33,34], enzymes [35,36], peptides [37], aptamers [38], antibody [39,40]. Electrochemical biosensors are considered as a reliable tool for infectious disease detection as they remain unaffected by sample absorbance or turbidity [41]. In order to increase the sensitivity of electrochemical biosensors, nanomaterials are often made use of as signal amplifiers such as graphene and AuNPs [42,43]. The electrical conductive properties of AuNPs have been extensively studied which enables them to improve the electronic transmission performance of sensors upon incorporation [44–46]. Moreover, since the synthesis of AuNPs is an easy one-step process and biocompatible for simple antibody physisorption conjugation, we have selected it as the signal amplification component in this research work.

In this study, we have fabricated FTO/AuNPs/SARS-CoV-2Ab electrode for the detection of SARS-CoV-2 Spike S1 Ag. The polyclonal SARS-CoV-2 Spike S1 Ab were raised in house and evaluated for its purity, and affinity for specific Ag by immunoassays. Here, FTO electrodes have been preferred over indium tin oxide (ITO) electrodes due to its high electrical conductivity, chemical stability, high tolerance towards physical abrasions and cost effectiveness [39]. Nanotechnology has played various roles in combating the SARS-CoV-2 pandemic [47] and in this research work, AuNPs were selected as the signal amplifiers due to their high conductivity, biocompatibility, stability, and ease of synthesis [48]. AuNPs were drop casted onto the FTO electrode and SARS-CoV-2 Spike S1 Ab was immobilised to detect the presence of SARS-CoV-2 Spike S1 Ag. All immobilization steps and optimisation of response time, antibody concentration, temperature, and pH were characterised using physicochemical methods such as UV–Vis Spectroscopy, Dynamic light Scattering Spectroscopy (DLS), Fourier Transform Infra-Red Spectroscopy (FT-IR), Cyclic Voltammetry (CV), Differential Pulse Voltammetry (DPV). The LOD of developed FTO based immunosensor was determined as 0.63 fM within the concentration range of 1 fM to 1 μM in standard buffer and 120 fM in case of spiked saliva samples. The fabricated immunosensor not only showed high sensitivity but also specificity towards SARS-CoV-2 Spike S1 Ag when compared with various other viral antigen (MERS Spike Ag, Avian Influenza Virus (AIV) Ag, and Human Immunodeficiency Virus (HIV) Ag), with a rapid response time of 10 s and stability up to 4 weeks. Hence, this immunosensor is a promising candidate for the development of rapid, non-invasive, specific, and sensitive detection of SARS-CoV-2 Spike S1 Ag directly from a patient's saliva sample.

2. Experimental section

2.1. Materials

Gold(III) chloride (Au_2Cl_6), Freund's complete adjuvant, and Freund's incomplete adjuvant were purchased from Sigma-Aldrich (India). Protein-A Sepharose resin was procured from Cytiva (Marlborough, USA). SARS-CoV-2 Ag (Spike S1 protein) was acquired from ProSci (California, USA). Human Immunodeficiency Virus (HIV) and Avian Influenza Virus (AIV) Ag were obtained from The Native Antigen Company (Oxford, UK). MERS Spike Ag was procured from R & D Systems (Minnesota, USA). Immobilon western chemiluminescent HRP Substrate (ECL) and polyvinylidene difluoride (PVDF) membrane were purchased from Merck Millipore (Darmstadt, Germany). 96-well NUNC microtiter plates for ELISA were acquired from Thermo Scientific (Bangalore, India). New Zealand white rabbit (7 weeks of age) was obtained from (Vyas Labs, Hyderabad) and housed at the small animal facility managed by the National institute of Animal Biotechnology (NIAB). All chemicals, solvents and reagents used were of high-quality analytical grade unless stated otherwise and all solutions were prepared in double distilled water.

2.2. Apparatus

ELISA readings were taken on ThermoFisher Scientific Multiskan™ FC Microplate Photometer (Bangalore, India) and SDS gel/Western Blot membrane imaging was done on ThermoFisher Scientific iBright™ CL1500 Imaging System (Bangalore, India). SDS-PAGE was run on BIORAD Mini-PROTEAN Tetra Vertical Electrophoresis Cell (Gurgaon, India) and semi-dry transfer of Western blot was carried out using BIORAD Trans-Blot Turbo Transfer System, (Gurgaon, India). UV–Vis and FT-IR spectra were acquired on Systonic S-924 Single-Beam UV–Vis Spectrophotometer (Delhi, India) and Thermo Scientific-Nicolet iS50 FT-IR (Bangalore, India) respectively. Changes in hydrodynamic diameter and zeta potential of each immobilization step were observed using Anton-Paar Litesizer 500 Particle Analyzer DLS (Gurgaon, India). CV and DPV measurements were performed with PalmSens4 (Netherlands). All experiments were performed at room temperature (RT) (25 °C) unless stated otherwise.

2.3. Immunization, purification, and characterization of SARS-CoV-2 spike S1Ab

2.3.1. Immunization and antibody production

7-weeks old New Zealand white rabbit was immunized subcutaneously with 180 μg of SARS CoV-2 Spike S1 recombinant protein emulsified with Freund's complete adjuvant. Subsequently, three boosters were given at 14-day intervals emulsified with Freund's incomplete adjuvant. The rabbit was bled and serum was separated on the 5th day after every booster to determine the Ab titre by Enzyme-Linked Immunosorbent Assay (ELISA). Anti-Spike S1

antibody was purified using Protein-A Sepharose following the product catalogue protocol (Protein A-Sepharose® CL-4B Cytiva). The purified fractions were pooled together and dialysed in Phosphate Buffer Saline (PBS) (pH 7.4).

2.3.2. Antibody characterization

The purity of the Ab was evaluated by electrophoresis and Western blot analysis. Purified SARS-CoV-2 Spike S1Ab was run on 12% sodium dodecyl sulphate polyacrylamide gel electrophoresis (SDS-PAGE) gel along with a protein ladder followed by staining and de-staining. For Western blot analysis, the SARS-CoV-2 Spike S1 Ag was run on 12% SDS-PAGE and the protein was transferred onto polyvinylidene difluoride (PVDF) membrane which was pre-activated for 5 min in methanol. The PVDF membrane was blocked using blocking buffer consisting of Bovine Serum Albumin (BSA) and skimmed milk in PBS (pH 7.4). PVDF membrane was further incubated with 1:8000 dilution of purified SARS-CoV-2 Spike S1Ab overnight at 4 °C and subsequently with Horse Radish Peroxidase (HRP) conjugated anti-rabbit secondary antibody at 1:10,000 dilution. The membrane was washed with PBS-Tween 20 (PBS-T) after each incubation step. Finally, enhanced chemiluminescence (ECL) was applied to the membrane and image was developed using ChemiDoc.

2.4. Immunoassay development

To further screen the specificity and binding of SARS-CoV-2 Spike S1 antibody, binding ELISA was performed in 96-well microtiter plates. ELISA plates were coated with 0.5 μg/mL SARS-CoV-2 Spike S1 antigen prepared in carbonate buffer (pH 9.6) and incubated overnight at 4 °C. Plate was washed with PBST (0.01%) and blocked for 1 h at 37 °C using 2% PBSM (2% skimmed milk in PBS). Plate was again washed, followed by addition of serially diluted SARS-CoV-2 Spike S1Ab and incubated for 2 h at 37 °C. Plate was washed and 1:10,000 dilution of secondary antibody solution was added (HRP labelled anti rabbit *anti*-IgG Ab) for 1 h at 37 °C. Plate was thoroughly washed as described previously and 3,3′,5,5′-Tetramethylbenzidine (TMB) substrate was added into each well. The colour was allowed to develop for 10 min and stopped using 1 N HCl (N = normality). Absorbance at 450 nm was measured using an ELISA plate reader.

From the above binding assay, the parameters and concentrations were standardised for competitive ELISA for SARS-CoV-2 Spike S1 Ag. The initial steps remained the same as the above indirect ELISA. After blocking and washing, different concentrations of Ag (SARS-CoV-2) were added to the plates, where 1°Ab concentration remained constant (2.5 μg/mL) and the Ag concentrations were serially diluted ranging from $1–1.9 \times 10^{-6}$ μg/mL. After 2 h incubation at 37 °C the remaining steps i.e. 2°Ab, washing, TMB and stop solution remain the same as above. Readings were taken at 450 nm in an ELISA plate reader.

2.5. Synthesis of AuNPs and its labelling with SARS-CoV-2Ab

AuNPs were synthesised using Turkevich [49] and Frens [50] heat-reflux citrate reduction method [51]. For synthesis of AuNPs, gold chloride (0.01 mL, 10%) was added to Milli-Q water and heated until mixture began to boil. 1 mL of 1% sodium citrate was immediately added to the boiling solution, that resulted in gradual change in the colour from yellow to dark blue and finally to wine red. The colloidal solution cooled and stored at 4 °C until further use. For labelling of SARS-CoV-2Ab with AuNPs, 90 μg SARS-CoV-2Ab was added dropwise to 1 mL of AuNPs solution in phosphate buffer saline (PB) (20 mM, pH 7.5) and incubated overnight (O/N) at 4 °C for further characterisation.

2.6. Characterisation of AuNPs and AuNPs/SARS-CoV-2Ab

Various physicochemical methods were used to confirm the labelling of SARS-CoV-2Ab with AuNPs. UV–Vis spectra were

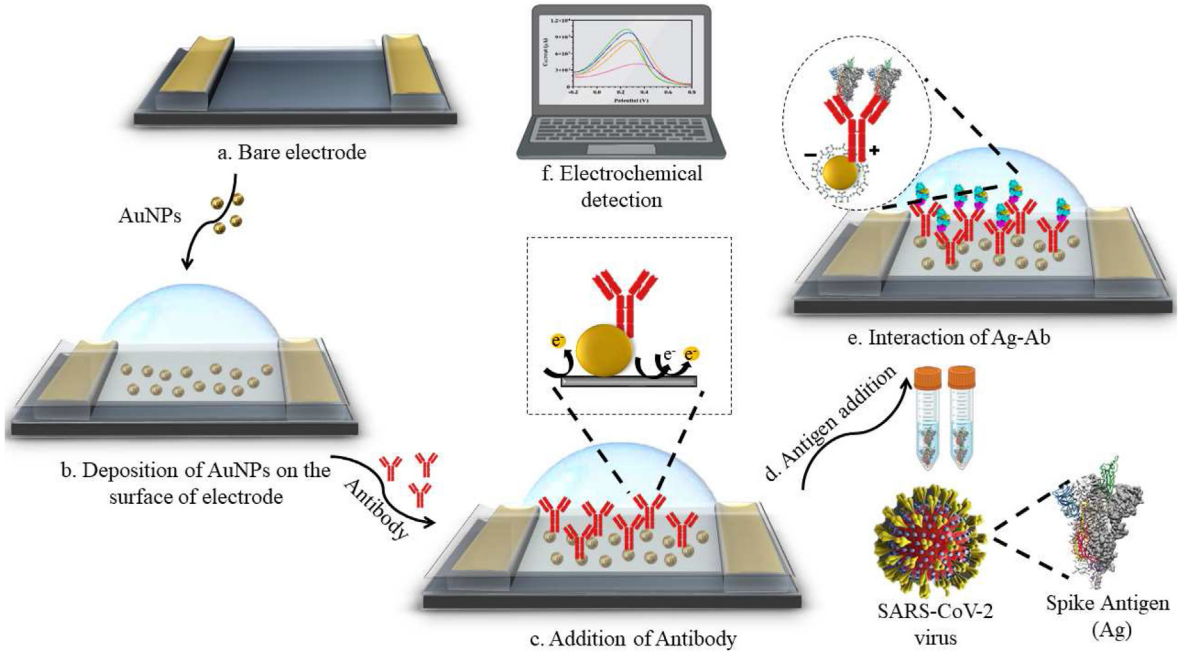

Scheme 1. Design of electrochemical Sensing. (a) Bare electrode; (b) Deposition of AuNPs on the surface of electrode; (c) Immobilization of SARS-CoV-2 Spike S1Ab on the surface of AuNPs via electrostatic or physisorption; (d) Addition of SARS-CoV-2 Spike S1 Ag, SARS-CoV-2 virus structure showing targeted surface protein i.e. Spike S1 Ag; (e) Interaction of Ag-Ab on the fabricated electrode that served as the working electrode in a 3 electrode system which consisted of Ag/AgCl as a reference electrode and platinum as a counter electrode; (f) Electrochemical detection to measure the binding interactions.

observed in the range of 200–800 nm for AuNPs and AuNPs/SARS-CoV-2Ab. The hydrodynamic diameter and zeta potential were obtained from DLS at 200 kHz. The hydrodynamic diameter calculated based on Stokes–Einstein equation as water was considered as the continuous phase (water viscosity = 0.911–0.852 mPa/s, diffusion coefficient of AuNPs = 6.89×10^{-9} to 5.30×10^{-8} cm^2/s) [48]. FT-IR spectra were taken in the range of 1000–4000 cm^{-1} to determine the changes in bonds/functional groups.

2.7. Fabrication, optimisation, and testing of FTO/AuNPs/SARS-CoV-2Ab with SARS-CoV-2 spike S1 Ag

100 μl of AuNPs were drop casted on the surface of FTO electrode and 100 μl of SARS-CoV-2Ab was immobilised. For, electrochemical characterisation Ag/AgCl was used as a reference electrode, and platinum as a counter electrode. This was done by sweeping the potential from −1.6 V to 1.8 V (CV) and −0.6 V–1.2 V (DPV) in $K_3[Fe(CN)_6]/K_4[Fe(CN)_6]$ solution. In order to confirm the conjugation of SARS-CoV-2Ab on the FTO electrode and obtain maximum sensing signal, various factors such as Ab concentration, response time, scan rate, pH, and temperature were optimised by comparing CV/DPV data. The SARS-CoV-2 Spike S1 Ag concentrations were prepared in the range 1 fM to 1 μM and LOD was determined. The application of the fabricated FTO/AuNPs/SARS-CoV-2Ab sensor was also evaluated for its degree of sensitivity in saliva samples spiked with SARS-CoV-2 spike S1 Ag. Furthermore, the stability and repeatability of the fabricated FTO/AuNPs/Ab electrode was also evaluated over a period of 4 weeks. The specificity was determined by analysing the cross-reactivity against other viral Ag of Middle East Respiratory Syndrome (MERS), Avian Influenza Virus (AIV), and Human Immunodeficiency Virus (HIV).

3. Results and discussion

3.1. Design and principle of the fabricated FTO/AuNPs/SARS-CoV-2Ab based immunosensor

Scheme 1 elucidates the mechanism of sensing and fabrication of the developed FTO immunosensor integrated with AuNPs and SARS-CoV-2Ab. AuNPs acted as a catalyst by providing large surface area for immobilization of Ab and also amplified the electrochemical signal by enhancement of electrical conductivity. Presence of AuNPs served as a platform for the attachment of SARS-CoV-2Ab by simple physisorption. Addition of SARS-CoV-2 Ag on

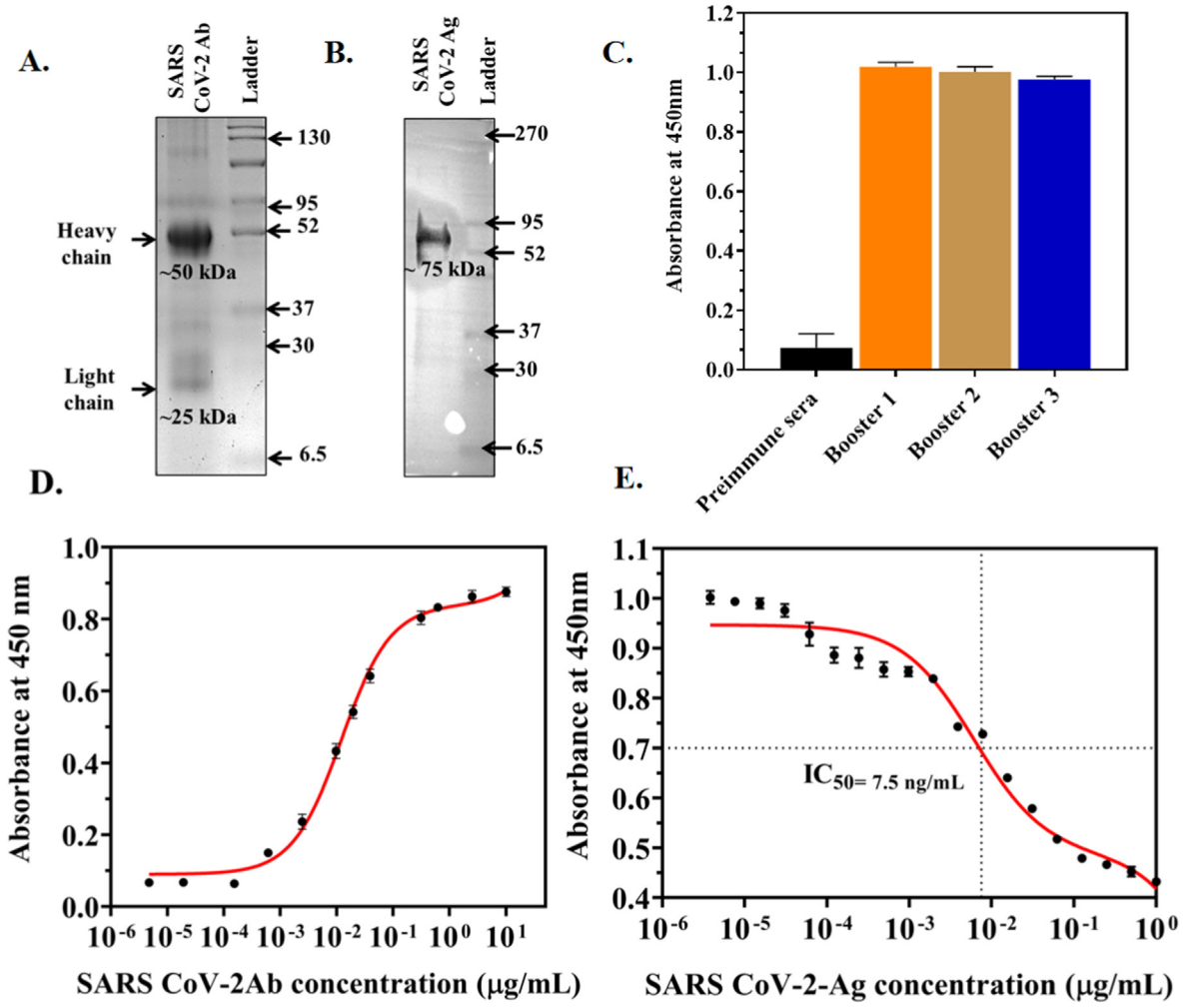

Fig. 1. Purification and characterisation of in-house SARS-CoV-2 Spike S1Ab. (A) SDS-PAGE gel image depicting both the heavy (50 kDa) and light (25 kDa) chains; (B) Western blot of SARS-CoV-2 Spike S1 Ag with molecular weight of 75 kDa; (C) Bar graph representing SARS-CoV-2 Spike S1Ab titre in pre-immune and booster serum; (D) Binding assay showing 0.25 μg/mL Ag and 2.5 μg/mL Ab as the optimum concentration for competitive ELISA; (E) Competitive ELISA titration curve to determine LOD of SARS-CoV-2 Spike S1 Ag with in-house developed SARS-CoV-2 Spike S1Ab.

FTO/AuNPs/SARS-CoV-2Ab led to a change in electrical current. The major phenomenon that lies behind is the orientation and polarity of the protein molecules that played a crucial role in the electron transfer from the electrode surface.

3.2. Characterization of SARS-CoV-2 spike S1 Ab and immunoassay development

Fig. 1 depicts the characterization of purified SARS-CoV-2 SpikeAb by SDS-PAGE, Western blot, and ELISA. The purified Ab revealed both the heavy (50 kDa) and light (25 kDa) chains after denaturation in SDS-PAGE (Fig. 1 A). The Western blot confirmed the binding of in-house produced Ab with the Ag (approximately 75 kDa) (Fig. 1 B). Antibody titer declined after 3rd booster as shown in Fig. 1C, hence the experiment was terminated at this point and final blood was collected. The generated Ab does not show any binding with pre immune sera in ELISA. The binding ELISA showed that 0.25 μg/mL Ag, and 2.5 μg/mL Ab were optimum to carry out competitive ELISA (Fig. 1 D). The limit of detection (LOD) for SARS-CoV-2 Spike S1 Ag competitive ELISA was determined as 7.5 ng/mL (Figure E).

3.3. Characterisation of AuNPs/SARS-CoV-2Ab complex

Fig. 2 A showed the characteristic peak of AuNPs at 520 nm due to its surface plasmon resonance (SPR) properties whereas a red shift of 9 nm was observed at 529 nm when AuNPs were labelled with SARS-CoV-2Ab due to an increase in the size of the complex that confirmed the immobilization of SARS-CoV-2Ab on the surface of AuNPs via electrostatic interactions or physisorption mechanism. Three additional peaks were observed in FT-IR spectra after conjugation of SARS-CoV-2Ab with AuNPs at 1290 cm^{-1} (C—O stretching) and 2564 cm^{-1} (S—H bond) and a new peak at 2328 cm^{-1} (C—N bond) which confirmed binding of AuNPs with SARS-CoV-2Ab (Fig. 2 B). These additional peaks corresponding to C—O, S—H and C—N bonds cannot be observed in native polyclonal IgG antibody graphs [52] and hence proves the conjugation of SARS-CoV-2Ab onto the AuNPs. The change in hydrodynamic diameter was also observed from 21 nm (bare AuNPs) to 30 ± 5 nm (AuNPs/SARS-CoV-2Ab) which further confirmed the conjugation of AuNPs with SARS-CoV-2Ab (Fig. 2C) as the size of the complex increased and the single and sharp peak showed that the particles are monodispersed in the colloidal solution. In Fig. 2 D, zeta potential shifted from −42 mV (bare AuNPs) to −39 mV (AuNPs/SARS-

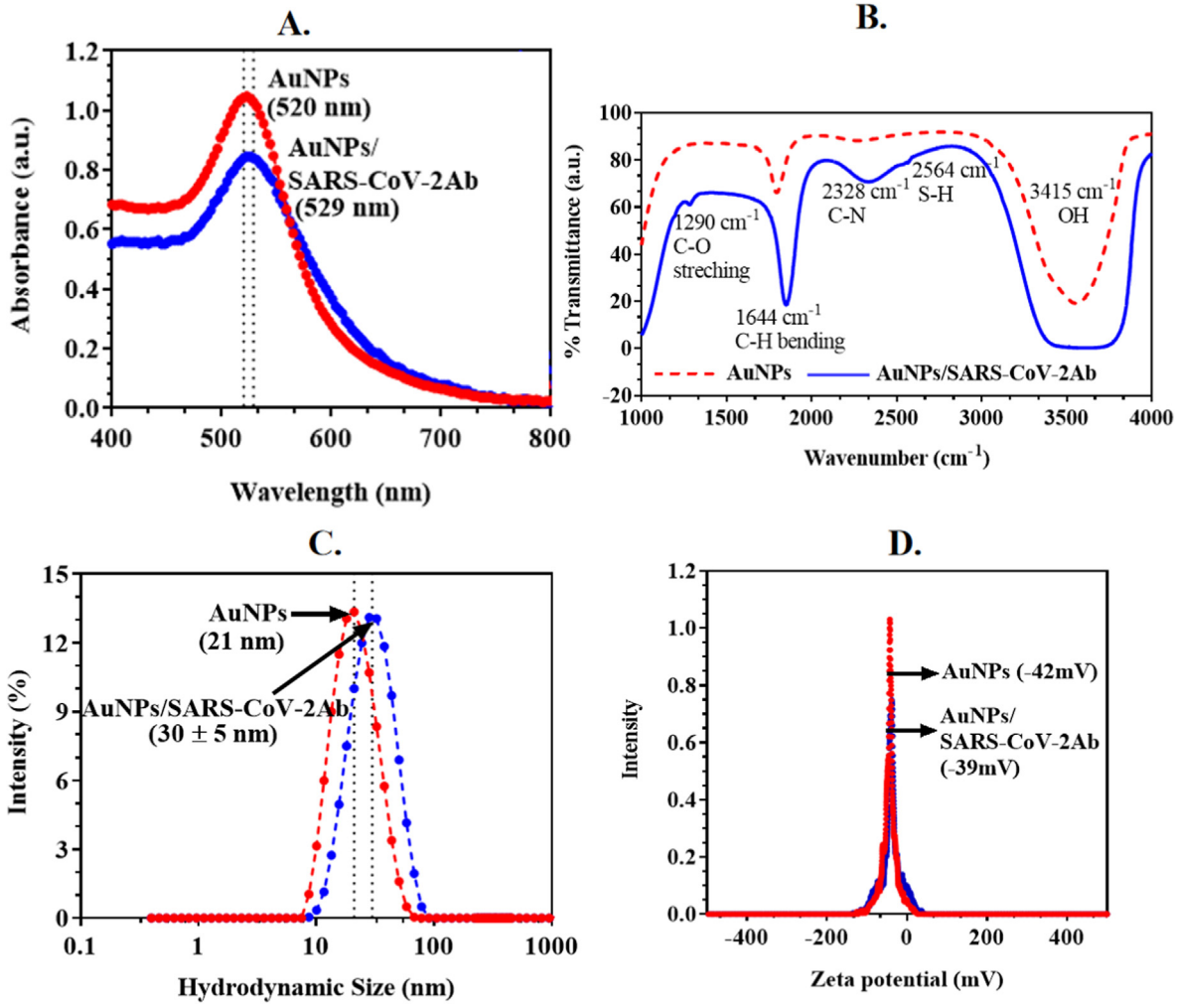

Fig. 2. Conjugation of SARS-CoV-2Ab on the surface of AuNPs. (A) The characteristic peak of bare AuNPs was observed at 520 nm due to SPR whereas the peak broadened and showed a red shift to 529 nm when AuNPs were labelled with SARS-CoV-2Ab. (B) In the FT-IR spectrum, three additional peaks were observed after conjugation of SARS-CoV-2Ab with AuNPs which included two small peaks at 1290 cm^{-1} (C—O stretching) and 2564 cm^{-1}(S—H bond) and a medium peak at 2328 cm^{-1} (C—N bond). (C) Hydrodynamic diameter increased from 21 nm to 30 ± 5 nm in case of the AuNPs/SARS-CoV-2Ab conjugate. (D) Zeta potential shifted from −42 mV (bare AuNPs) to −39 mV (AuNPs/SARS-CoV-2Ab). (For interpretation of the references to colour in this figure legend, the reader is referred to the Web version of this article.)

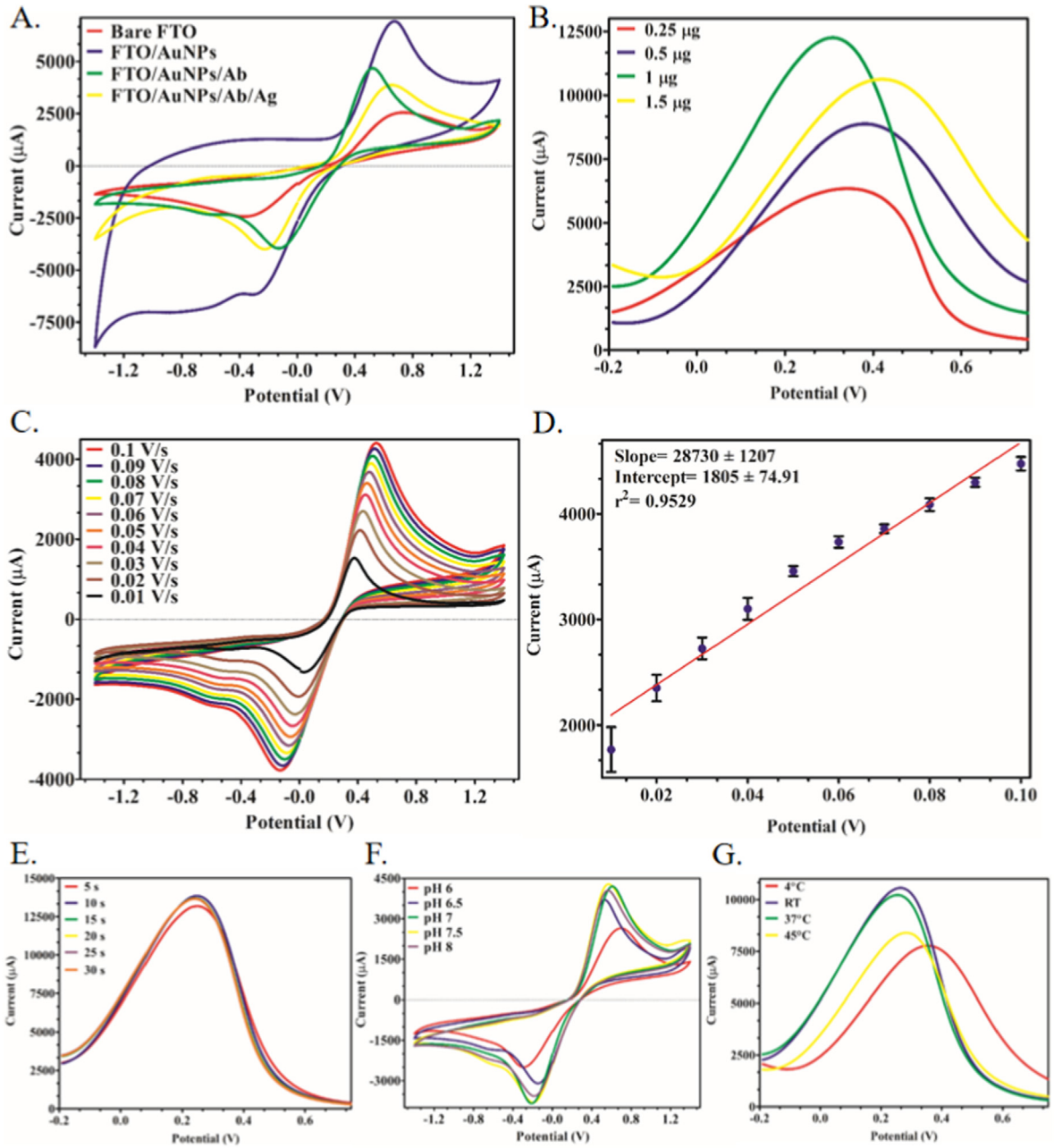

Fig. 3. Optimisation of the fabricated FTO electrode in the scanning potential range of −1.4 V to 1.4 V (CV) and −0.0.5 to 1.0 (DPV): (A) CV spectra of bare FTO, FTO/AuNPs, FTO/AuNPs/SARS-CoV-2Ab, and FTO/AuNPs/SARS-CoV-2Ab/Ag; (B) DPV spectra of different concentrations of SARS-CoV-2Ab (0.25–1.5 µg) with highest current output at 1.0 µg SARS-CoV-2Ab; (C) CV of different scan rates ranging from 0.1 V/s to 0.01 V/s showed decrease in current output with decrease in scan rate; (D) Calibration curve of scan rate CV spectra; (E) DPV spectra of different response time (5 s–30 s) were superimposed with stable current output at 10 s and beyond; (F) CV at five different pH (6, 6.5, 7, 7.5, 8) where pH 7.5 inferred the highest current followed by pH 7; (G) DPV spectra at four different temperatures (4 °C, RT, 37 °C, 45 °C) showed maximum current output at RT followed by 37 °C.

CoV-2Ab) due to insulating effect of SARS-CoV-2Ab.

3.4. Optimisation of fabricated FTO/AuNPs/SARS-CoV-2Ab based immunosensor

The electrochemical parameters were optimised for better performance of the electrode as shown in Fig. 3. A huge spike in the current was observed in Fig. 3 A after immobilization of AuNPs onto bare FTO electrodes due to high conductivity of AuNPs that accelerates the electron transfer from the surface of electrode [29]. Addition of Ab onto the AuNPs led to a drop in the current which further decreased on addition of Ag due to the masking effect posed by proteins. The analytical performance of the modified FTO/AuNPs electrode was optimised where different concentrations of Ab (0.25–1.5 µg) were analysed with highest current observed at 1.0 µg (Fig. 3 B) as further increase in concentration of Ab would lead to masking of the conductive surface. CV spectra of different scan rates were recorded from 0.1 V/s to 0.01 V/s (Fig. 3C), which showed an increase in current output with increase in the scan rate. The calibration curve of the scan rate graph (Fig. 3 D) was plotted to give an

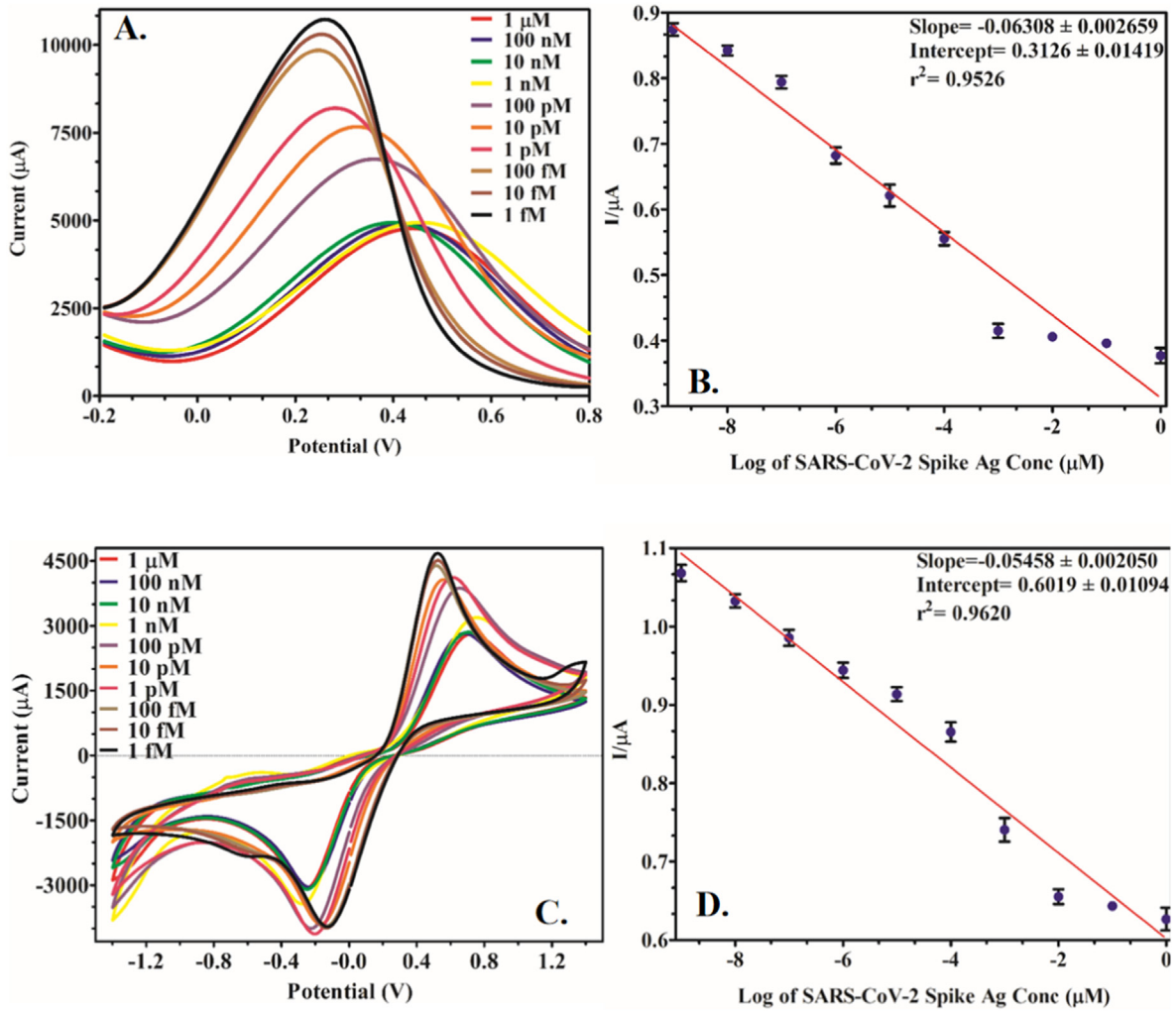

Fig. 4. DPV and CV of different concentrations of SARS-CoV-2 Ag on the fabricated FTO/AuNPs/SARS-CoV-2Ab electrode in the scanning potential range of −1.4 V to 1.4 V and −0.5 V–1.0 V respectively: (A) DPV at different concentrations of SARS-CoV-2 Ag (1 μM, 100 nM, 10 nM, 1 nM, 100 pM, 10 pM, 1 pM, 100 fM, 10 fM, 1 fM); (B) Standard calibration curve between log of the various concentrations of SARS-CoV-2 Ag; (C) CV at different concentrations of SARS-CoV-2 Ag (1 μM, 100 nM, 10 nM, 1 nM, 100 pM, 10 pM, 1 pM, 100 fM, 10 fM, 1 fM); (D) Standard calibration curve between log of the various concentrations of SARS-CoV-2 Ag.

r^2 value of 0.9529. The maximum response time was seen at 10 s and beyond at which point all binding sites in SARS-CoV-2Ab were saturated with SARS-CoV-2 Ag (Fig. 3 E). The optimum pH required for maximum current signal at different pH range (6.0, 6.5, 7.0, 7.5, 8.0) was tested, with maximum signal obtained at pH 7.5 as well as 7.0 (Fig. 3 F). Therefore, buffer with pH 7.4 (PB) was used as the optimum pH for further detection experiments. The electrode performance was also recorded at different temperatures (4 °C, RT, 37 °C, 45 °C) (Fig. 3 G) with maximum current output seen at RT followed by at 37 °C as this is the ideal temperature for antigen-antibody action. Hence all further experiments were carried out at RT which is the ideal temperature for physiological samples.

3.5. Analytical performance of the fabricated FTO/AuNPs/Ab electrode

Both DPV and CV were used for the determination of SARS-CoV-2 spike S1 Ag concentration as shown in Fig. 4 A and C. With increasing SARS-CoV-2 spike S1 Ag concentration, the current kept decreasing due to the masking effect of addition of protein. The linear regression equation for DPV is explained in (Fig. 4 B): the intercept and slope are 0.3126 ± 0.01419 and −0.06308 ± 0.002659 respectively with r^2 = 0.9526. Similarly, the linear regression equation for CV is explained in (Fig. 4 D): the intercept and slope are 0.6019 ± 0.01094 and −0.05458 ± 0.002050 respectively with r^2 = 0.9620. Different concentrations of SARS-CoV-2 Ag ranging from 1 fM to 1 μM (standard buffer 1 X PB pH 7.4) were tested on the FTO/AuNPs/SARS-CoV-2Ab modified electrodes and the standard calibration curve was plotted based on DPV (Fig. 4 B) which gave the LOD as 0.63 fM for SARS-CoV-2 Ag using formula $3(S_y/S)$, where S_y corresponds to the standard deviation of the response and S corresponds to the slope of the calibration curve. Since the developed immunosensor can detect the Ag at femtomolar levels, it is highly sensitive as compared to other diagnostic techniques available for SARS-CoV-2 (Table 1), which gives it an advantage in case of low titre levels of the virus. Similarly, the standard calibration curve was plotted based on CV as well (Fig. 4 D).

Cross reactivity studies were done to test non-specific binding of other viral Ag as shown in Fig. 5 A that showed decrease in peak current with SARS-CoV-2 Ag whereas no change in peak current was observed with Middle East Respiratory Syndrome (MERS), Avian Influenza Virus (AIV), and Human Immunodeficiency Virus

Table 1
Currently available diagnostic techniques for detection of SARS-CoV-2.

Type of Test	Institute	Limit of Detection	Reference
Virus blood culture and high-throughput sequencing of the whole genome	Wuhan Institute of Virology	Not Available	[53]
Real time RT-PCR	Charité – Universitätsmedizin Berlin Institute of Virology	3.9 copies per reaction for the E[a] gene assay 3.6 copies per reaction for the RdRp[b] assay	[13]
High Resolution CT (HRCT)	Huazhong University of Science and Technology	Not Available	[54]
Mass Spectrometric Identification	Martin Luther University	10^{e}–10^{f} genome equivalents/μL	[55]
All-in-One Dual (DNA and RNA) CRISPR[c]-Cas12a (AIOD-CRISPR) Assay	University of Connecticut Health Center	1.2 copies DNA targets and 4.6 copies RNA targets	[23]
CRISPR-Cas 12 (CRISPR associated 12) portable assay	CASPR Biotech	10^{c} copies/mL	[56]
CRISPR-Cas 12 based LFA[d]	University of California, Mammoth Biosciences	10 copies/μL	[57]
CRISPR Cas12a/gRNA complex fluorescent probe assay	Tulane University School of Medicine	2 copies/mL	[58]
Rapid IgM-IgG combined Ab test kit	Guangzhou Medical University	Not Available	[22]
Closed tube one stage LAMP[e]	University of Pennsylvania	Not Available	[59]
Closed tube two stage isothermal amplification RAMP[f] assay	University of Pennsylvania	Not Available	[59]
RNA based paper LFA PoC diagnostic device using LAMP assay	National Tsing Hua University	Not Available	[24]
RT-LAMP colorimetric assay	University of Oxford	80 copies viral RNA/mL	[60]
RT-LAMP assay	National University College of Medicine and Medical Research Institute, Cheongju	10^{b} RNA copies	[61]
Colorimetric LAMP assay	Washington University	~10^{b} viral genome/reaction	[62]
ELISA[g] and gold immunochromatographic assay (GICA) for combined IgG-IgM	Wuhan University	Not Available	[18]
Field Effect Transistor- based electrochemical biosensor	Korea Basic Science Institute	1.6×10^{1} pfu/mL (culture medium) 2.42×10^{2} copies/mL (clinical samples)	[20]
Dual Functional Plasmonic Photothermal Biosensor	Institute of Environmental Engineering, ETH Zürich	0.22 pM	[63]
Portable Surface Plasmon Resonance Sensing	Université de Montréal	~1 μg/mL	[64]
Gold nanoparticle based colorimetric assay	University of Maryland	0.18 ng/μL	[65]
Potentiostat based FTO immunosensor	National Institute of Animal Biotechnology	0.63 fM (buffer) 120 fM (saliva)	Current research work

[a] Envelope.
[b] RNA-dependant RNA polymerase.
[c] Clusters of Regularly Interspaced Short Palindromic Repeats.
[d] Lateral flow assay.
[e] Loop-mediated isothermal amplification.
[f] Rapid analyte measurement platform.
[g] Enzyme-linked immunosorbent assay.

(HIV) similar to the blank FTO/AuNPs/SARS-CoV-2Ab electrode peak current when all Ag concentrations were kept constant at 1 μM. This showed the high specificity of the SARS-CoV-2Ab towards SARS-CoV-2 Ag and in turn the sensor. Furthermore, repeatability and stability parameters were also evaluated for FTO/AuNPs/SARS-CoV-2Ab fabricated electrode. In this case, multiple readings of saliva samples spiked with SARS-CoV-2 Ag were taken on a single modified electrode (Fig. 5 B). The results indicated that each individual electrode could be used up to 3–4 times without major changes in the peak current and could detect up to 120 fM (LOD in spiked saliva sample). After the 5th time, most of the immobilised Ab on the surface of the FTO may have been removed due to multiple washing rounds and hence the drop is current was observed. The stability of the FTO/AuNPs/SARS-CoV-2Ab fabricated electrode was observed at 7th, 14th, 21st and 28th day of its fabrication and stored at 4 °C. In Fig. 5C, the modified electrode provided stable readings over a period of three weeks i.e. 21 days and only a slight dip in signal was seen after the 4th week i.e. 28 days which proved the electrode could be stored at 4 °C up to 28 days and used for testing samples in a laboratory set up for up to 4 weeks without any compromise in results as the activity of the immobilised Ab on the FTO surface remained the same when stored at 4 °C.

4. Conclusion

In this proposed work, we have successfully developed FTO/AuNPs/SARS-CoV-2Ab modified electrode for the rapid detection of SARS-CoV-2 spike S1 protein with LOD of 0.63 fM in standard buffer and 120 fM in spiked saliva samples. The fabricated electrode showed no cross reactivity with other viral Ag, provide a rapid response in 10 s, with a storage shelf life for up to 4 weeks. The fabricated electrode can further be potentially used directly on clinical patient saliva samples for non-invasive SARS-CoV-2 diagnostics. The only drawback of this sensor is the requirement of a potentiostat for reading the electrode which may require a lab set up and a technician. However, it is easy to fabricate and does not require as much time as the gold standard RT-PCR technique and with the current rise in cases, time taken to get a result is crucial. The developed biosensor can detect even trace amounts of spike S1 protein in spiked saliva at femtomolar levels. Moreover, since the bioreceptor component of the electrode, SARS-CoV-2 spike S1 Ab, was produced in-house, the overall cost of the electrode fabrication was reduced substantially making it a cheaper alternative. The electrode also shows great future research potential for miniaturisation as well as detection of various other diseases since the sensor can easily be customised by immobilising any bioreceptor onto the AuNPs, specific to a particular target analyte.

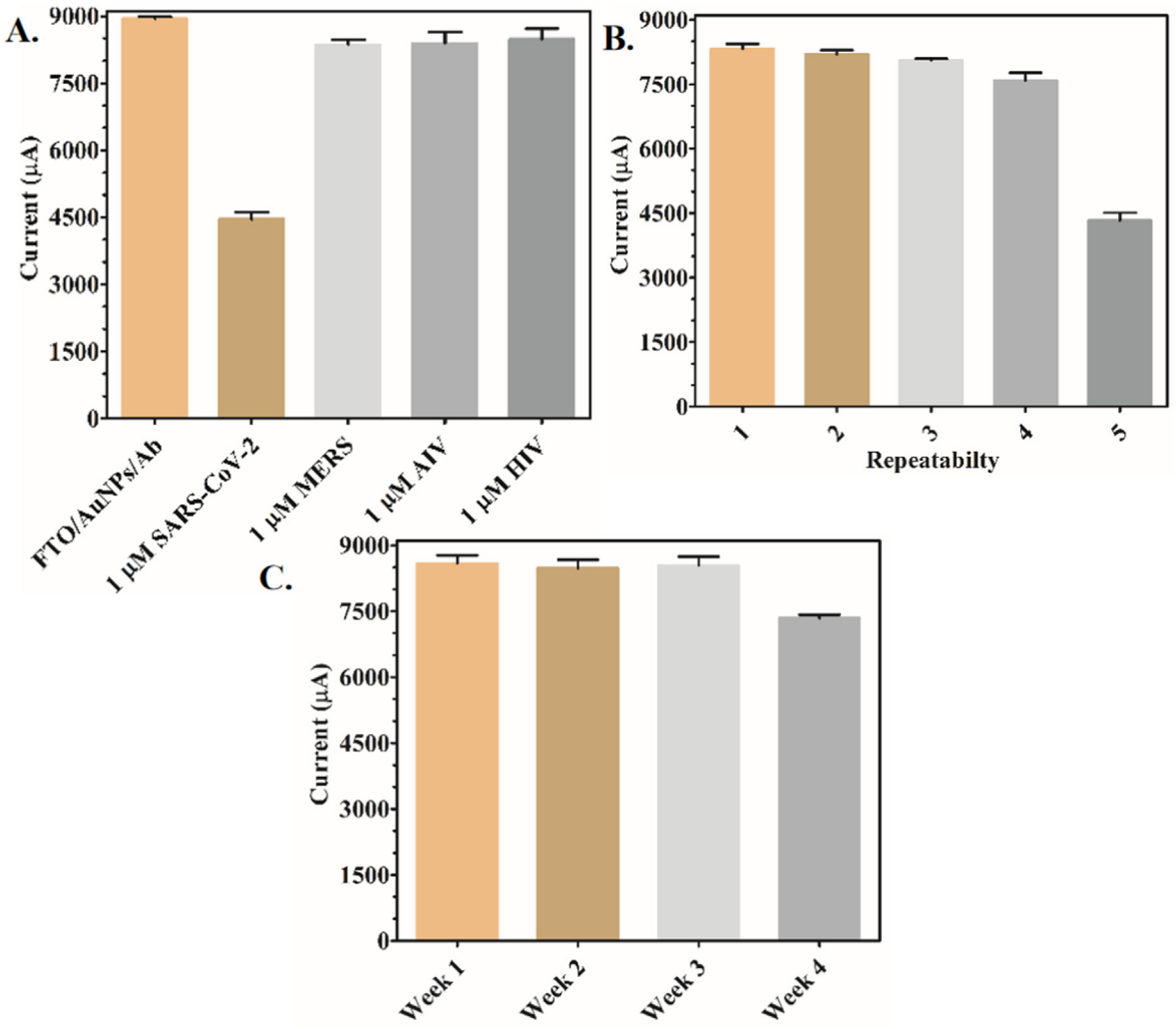

Fig. 5. Specificity, repeatability and stability testing of fabricated FTO/AuNPs/SARS-CoV-2Ab electrode in the scanning potential range of −1.4 V to 1.4 V and −0.5 V−1.0 V respectively: (A) Cross reactivity studies with MERS, AIV, and HIV Ag; (B) Repeatability of individual fabricated FTO/AuNPs/SARS-CoV-2Ab electrodes tested multiple times on saliva samples spiked with 120 fM concentration of SARS-CoV-2 Ag; (C) Stability of fabricated electrode tested over a period of 4 weeks at 7 day time intervals.

Author contribution statement

Sonu Gandhi: Conceptualization, Supervision, Visualization, Writing– review, Funding acquisition, Project administration. **Akanksha Roberts:** Writing original draft, review and editing, Experimentation, Investigation, Analysis. **Subhasis Mahari:** Experimentation, Investigation, Analysis, Writing original draft, review and editing. **Deepshikha Shahdeo:** Writing, Experimentation, Investigation, Analysis, Writing original draft, review and editing.

Animal ethics approval

All animal related experiments were conducted at Small Animal Facility, National Institute of Animal Biotechnology, Hyderabad after due approval from the Institutional Animal Ethics Committee (IAEC) with approval number IAEC/2020/NIAB/04/SG.

Declaration of competing interest

The authors declare that they have no known competing financial interests or personal relationships that could have appeared to influence the work reported in this paper.

Acknowledgements

We are grateful for the research endowment under the Intensification of Research in High Priority Area (IRHPA) program from Science and Engineering Research Board (SERB), New Delhi (Grant Number IPA/2020/000069). The authors would like to thank Dr. Jayant Hole for providing support during animal experimentation. A.R. would like to acknowledge DST-INSPIRE fellowship (IF180729) sponsored by the Department of Science and Technology (DST), New Delhi and S.M. would like to acknowledge CSIR Fellowship (09/1150(0013)/2019/EMR-I) provided by the Council of Scientific and Industrial Research (CSIR), New Delhi.

References

[1] G. Li, Y. Fan, Y. Lai, T. Han, Z. Li, P. Zhou, P. Pan, W. Wang, D. Hu, X. Liu, Q. Zhang, J. Wu, Coronavirus infections and immune responses, J. Med. Virol. 92 (2020) 424–432.
[2] N. Zhu, D. Zhang, W. Wang, X. Li, B. Yang, J. Song, X. Zhao, B. Huang, W. Shi, R. Lu, P. Niu, F. Zhan, X. Ma, D. Wang, W. Xu, G. Wu, G.F. Gao, W. Tan, A novel coronavirus from patients with pneumonia in China, 2019, N. Engl. J. Med. 382 (2020) 727–733.
[3] F. Wu, S. Zhao, B. Yu, Y.M. Chen, W. Wang, Z.G. Song, Y. Hu, Z.W. Tao, J.H. Tian, Y.Y. Pei, M.L. Yuan, Y.L. Zhang, F.H. Dai, Y. Liu, Q.M. Wang, J.J. Zheng, L. Xu, E.C. Holmes, Y.Z. Zhang, A new coronavirus associated with human respiratory disease in China, Nature 579 (2020) 265–269.

[4] L. Chen, W. Liu, Q. Zhang, K. Xu, G. Ye, W. Wu, Z. Sun, F. Liu, K. Wu, B. Zhong, Y. Mei, W. Zhang, Y. Chen, Y. Li, M. Shi, K. Lan, Y. Liu, RNA based mNGS approach identifies a novel human coronavirus from two individual pneumonia cases in 2019 Wuhan outbreak, Emerg, Microb. Infect. 9 (2020) 313–319.
[5] L.-L. Ren, Y.-M. Wang, Z.-Q. Wu, Z.-C. Xiang, L. Guo, T. Xu, Y.-Z. Jiang, Y. Xiong, Y.-J. Li, X.-W. Li, H. Li, G.-H. Fan, X.-Y. Gu, Y. Xiao, H. Gao, J.-Y. Xu, F. Yang, X.-M. Wang, C. Wu, L. Chen, Y.-W. Liu, B. Liu, J. Yang, X.-R. Wang, J. Dong, L. Li, C.-L. Huang, J.-P. Zhao, Y. Hu, Z.-S. Cheng, L.-L. Liu, Z.-H. Qian, C. Qin, Q. Jin, B. Cao, J.-W. Wang, Identification of a novel coronavirus causing severe pneumonia in human, Chin. Med. J. 133 (2020) 1015–1024.
[6] J.F.W. Chan, S. Yuan, K.H. Kok, K.K.W. To, H. Chu, J. Yang, F. Xing, J. Liu, C.C.Y. Yip, R.W.S. Poon, H.W. Tsoi, S.K.F. Lo, K.H. Chan, V.K.M. Poon, W.M. Chan, J.D. Ip, J.P. Cai, V.C.C. Cheng, H. Chen, C.K.M. Hui, K.Y. Yuen, A familial cluster of pneumonia associated with the 2019 novel coronavirus indicating person-to-person transmission: a study of a family cluster, Lancet 395 (2020) 514–523.
[7] H.X. Bai, B. Hsieh, Z. Xiong, K. Halsey, J.W. Choi, T.M.L. Tran, I. Pan, L.-B. Shi, D.-C. Wang, J. Mei, X.-L. Jiang, Q.-H. Zeng, T.K. Egglin, P.-F. Hu, S. Agarwal, F. Xie, S. Li, T. Healey, M.K. Atalay, W.-H. Liao, Performance of radiologists in differentiating COVID-19 from viral pneumonia on chest CT, Radiology 296 (2020) E46–E54.
[8] A. Bernheim, X. Mei, M. Huang, Y. Yang, Z.A. Fayad, N. Zhang, K. Diao, B. Lin, X. Zhu, K. Li, S. Li, H. Shan, A. Jacobi, M. Chung, Chest CT findings in coronavirus disease-19 (COVID-19): relationship to duration of infection, Radiology 295 (2020) 685–691.
[9] Y. Li, L. Xia, Coronavirus disease 2019 (COVID-19): role of chest CT in diagnosis and management, Am. J. Roentgenol. (2020) 1–7.
[10] F. Pan, T. Ye, P. Sun, S. Gui, B. Liang, L. Li, D. Zheng, J. Wang, R.L. Hesketh, L. Yang, C. Zheng, Time course of lung changes on chest CT during recovery from 2019 novel coronavirus (COVID-19) pneumonia, Radiology 295 (2020) 715–721.
[11] L. Lan, D. Xu, G. Ye, C. Xia, S. Wang, Y. Li, H. Xu, Positive RT-PCR test results in patients recovered from COVID-19, JAMA, J. Am. Med. Assoc. 323 (2020) 1502–1503.
[12] D.K.W. Chu, Y. Pan, S.M.S. Cheng, K.P.Y. Hui, P. Krishnan, Y. Liu, D.Y.M. Ng, C.K.C. Wan, P. Yang, Q. Wang, M. Peiris, L.L.M. Poon, Molecular diagnosis of a novel coronavirus (2019-nCoV) causing an outbreak of pneumonia, Clin. Chem. 66 (2020) 549–555.
[13] V.M. Corman, O. Landt, M. Kaiser, R. Molenkamp, A. Meijer, D.K. Chu, T. Bleicker, S. Brünink, J. Schneider, M.L. Schmidt, D.G. Mulders, B.L. Haagmans, B. van der Veer, S. van den Brink, L. Wijsman, G. Goderski, J.L. Romette, J. Ellis, M. Zambon, M. Peiris, H. Goossens, C. Reusken, M.P. Koopmans, C. Drosten, Detection of 2019 novel coronavirus (2019-nCoV) by real-time RT-PCR, Euro Surveill. 25 (2020) 2000045–2000053.
[14] M.J. Loeffelholz, Y.-W. Tang, Laboratory diagnosis of emerging human coronavirus infections — the state of the art, Emerg. Microb. Infect. 9 (2020) 747–756.
[15] T. Ai, Z. Yang, H. Hou, C. Zhan, C. Chen, W. Lv, Q. Tao, Z. Sun, L. Xia, Correlation of chest CT and RT-PCR testing in coronavirus disease 2019 (COVID-19) in China: a report of 1014 cases, Radiology 296 (2020) 32–40.
[16] Y. Fang, H. Zhang, J. Xie, M. Lin, L. Ying, P. Pang, W. Ji, Sensitivity of chest CT for COVID-19: comparison to RT-PCR, Radiology 296 (2020) E115–E117.
[17] A. Parihar, P. Ranjan, S.K. Sanghi, A.K. Srivastava, R. Khan, Point-of-Care biosensor-based diagnosis of COVID-19 holds promise to combat current and future pandemics, ACS Appl. Bio Mater. 3 (2020) 7326–7343.
[18] J. Xiang, M. Yan, H. Li, T. Liu, C. Lin, S. Huang, C. Shen, Evaluation of enzyme-linked immunoassay and colloidal gold- immunochromatographic assay kit for detection of novel coronavirus (SARS-Cov-2) causing an outbreak of pneumonia (COVID-19), MedRxiv (2020), https://doi.org/10.1101/2020.02.27.20028787.
[19] S. Yadav, M.A. Sadique, P. Ranjan, N. Kumar, A. Singhal, A.K. Srivastava, R. Khan, SERS based lateral flow immunoassay for point-of-care detection of SARS-CoV-2 in clinical samples, ACS Appl. Bio Mater. 4 (2021) 2974–2995.
[20] G. Seo, G. Lee, M.J. Kim, S.-H. Baek, M. Choi, K.B. Ku, C.-S. Lee, S. Jun, D. Park, H.G. Kim, S.-J. Kim, J.-O. Lee, B.T. Kim, E.C. Park, S. Il Kim, Rapid detection of COVID-19 causative virus (SARS-CoV-2) in human nasopharyngeal swab specimens using field-effect transistor-based biosensor, ACS Nano 14 (2020) 5135–5142.
[21] M. Abubakar Sadique, S. Yadav, P. Ranjan, M. Akram Khan, A. Kumar, R. Khan, Rapid detection of SARS-CoV-2 using graphene-based IoT integrated advanced electrochemical biosensor, Mater. Lett. 305 (2021), 130824.
[22] Z. Li, Y. Yi, X. Luo, N. Xiong, Y. Liu, S. Li, R. Sun, Y. Wang, B. Hu, W. Chen, Y. Zhang, J. Wang, B. Huang, Y. Lin, J. Yang, W. Cai, X. Wang, J. Cheng, Z. Chen, K. Sun, W. Pan, Z. Zhan, L. Chen, F. Ye, Development and clinical application of a rapid IgM-IgG combined antibody test for SARS-CoV-2 infection diagnosis, J. Med. Virol. 92 (2020) 1518–1524.
[23] X. Ding, K. Yin, Z. Li, C. Liu, All-in-One dual CRISPR-cas12a (AIOD-CRISPR) assay: a case for rapid, ultrasensitive and visual detection of novel coronavirus SARS-CoV-2 and HIV virus, BioRxiv 11 (2020) 4711–4730, https://doi.org/10.1101/2020.03.19.998724.
[24] T. Yang, Y.-C. Wang, C.-F. Shen, C.-M. Cheng, Point-of-Care RNA-based diagnostic device for COVID-19, Diagnostics 10 (2020) 165–168.
[25] A. Kasoju, D. Shahdeo, A.A. Khan, N.S. Shrikrishna, S. Mahari, A.M. Alanazi, M.A. Bhat, J. Giri, S. Gandhi, Fabrication of microfluidic device for Aflatoxin M1 detection in milk samples with specific aptamers, Sci. Rep. 10 (2020) 1–8.
[26] S. Gandhi, I. Banga, P.K. Maurya, S.A. Eremin, A gold nanoparticle-single-chain fragment variable antibody as an immunoprobe for rapid detection of morphine by dipstick, RSC Adv. 8 (2018) 1511–1518.
[27] P. Mishra, I. Banga, R. Tyagi, T. Munjal, A. Goel, N. Capalash, P. Sharma, C.R. Suri, S. Gandhi, An immunochromatographic dipstick as an alternate for monitoring of heroin metabolites in urine samples, RSC Adv. 8 (2018) 23163–23170.
[28] S. Singh, P. Mishra, I. Banga, A.S. Parmar, P.P. Tripathi, S. Gandhi, Chemiluminescence based immunoassay for the detection of heroin and its metabolites, Bioimpacts 8 (2017) 53–58.
[29] J.N. Tey, S. Gandhi, I.P.M. Wijaya, A. Palaniappan, J. Wei, I. Rodriguez, C.R. Suri, S.G. Mhaisalkar, Direct detection of heroin metabolites using a competitive immunoassay based on a carbon-nanotube liquid-gated field-effect transistor, Small 6 (2010) 993–998.
[30] R.G. Kerry, S. Malik, Y.T. Redda, S. Sahoo, J.K. Patra, S. Majhi, Nano-based approach to combat emerging viral (NIPAH virus) infection, Nanomed. Nanotechnol. Biol. Med. 18 (2019) 196–220.
[31] A. Roberts, S. Gandhi, Japanese encephalitis virus: a review on emerging diagnostic techniques, Front. Biosci. - Landmark 25 (2020) 1875–1893.
[32] A. Roberts, N. Chauhan, S. Islam, S. Mahari, B. Ghawri, R.K. Gandham, S.S. Majumdar, A. Ghosh, S. Gandhi, Graphene functionalized field-effect transistors for ultrasensitive detection of Japanese encephalitis and Avian influenza virus, Sci. Rep. 10 (2020) 14546.
[33] J. Labuda, R. Ovádeková, J. Galandová, DNA-based biosensor for the detection of strong damage to DNA by the quinazoline derivative as a potential anti-cancer agent, Microchim. Acta. 164 (2009) 371–377.
[34] T. Jiang, M. Minunni, P. Wilson, J. Zhang, A.P.F. Turner, M. Mascini, Detection of TP53 mutation using a portable surface plasmon resonance DNA-based biosensor, Biosens. Bioelectron. 20 (2005) 1939–1945.
[35] R. Ilangovan, D. Daniel, A. Krastanov, C. Zachariah, R. Elizabeth, Enzyme based biosensor for heavy metal ions determination, Biotechnol. Biotechnol. Equip. 20 (2006) 184–189.
[36] S. Jawaheer, S.F. White, S.D.D.V. Rughooputh, D.C. Cullen, Development of a common biosensor format for an enzyme based biosensor array to monitor fruit quality, Biosens. Bioelectron. 18 (2003) 1429–1437.
[37] S. Gandhi, H. Arami, K.M. Krishnan, Detection of cancer-specific proteases using magnetic relaxation of peptide-conjugated nanoparticles in biological environment, Nano Lett. 16 (2016) 3668–3674.
[38] A. Kasoju, N.S. Shrikrishna, D. Shahdeo, A.A. Khan, A.M. Alanazi, S. Gandhi, Microfluidic paper device for rapid detection of aflatoxin B1 using an aptamer based colorimetric assay, RSC Adv. 10 (2020) 11843–11850.
[39] A. Roberts, P.P. Tripathi, S. Gandhi, Graphene nanosheets as an electric mediator for ultrafast sensing of urokinase plasminogen activator receptor-A biomarker of cancer, Biosens. Bioelectron. 141 (2019) 111398.
[40] S. Islam, S. Shukla, V.K. Bajpai, Y.-K. Han, Y.S. Huh, A. Kumar, A. Ghosh, S. Gandhi, A smart nanosensor for the detection of human immunodeficiency virus and associated cardiovascular and arthritis diseases using functionalized graphene-based transistors, Biosens. Bioelectron. 126 (2019) 792–799.
[41] E. Bakker, Electrochemical sensors, Anal. Chem. 76 (2004) 3285–3298.
[42] J.M. Pingarrón, P. Yáñez-Sedeño, A. González-Cortés, Gold nanoparticle-based electrochemical biosensors, Electrochim. Acta 53 (2008) 5848–5866.
[43] D. Shahdeo, A. Roberts, N. Abbineni, S. Gandhi, Graphene based sensors, in: Compr. Anal. Chem., 2020, pp. 175–199. Elsevier B.V.
[44] M.J. Tommalieh, A.M. Ismail, N.S. Awwad, H.A. Ibrahium, M.A. Youssef, A.A. Menazea, Investigation of electrical conductivity of gold nanoparticles scattered in polyvinylidene fluoride/polyvinyl chloride via laser ablation for electrical applications, J. Electron. Mater. 49 (2020) 7603–7608.
[45] D. Coetzee, M. Venkataraman, J. Militky, M. Petru, Influence of nanoparticles on thermal and electrical conductivity of composites, Polymers 12 (2020) 742–766.
[46] Y. Zhang, A.M. Schwartzberg, K. Xu, C. Gu, J.Z. Zhang, Electrical and thermal conductivities of gold and silver nanoparticles in solutions and films and electrical field enhanced Surface-Enhanced Raman Scattering (SERS), Phys. Chem. Interfaces Nanomater. IV. 5929 (2005), 592912.
[47] M.A. Sadique, S. Yadav, P. Ranjan, S. Verma, S.T. Salammal, M.A. Khan, A. Kaushik, R. Khan, High-performance antiviral nano-systems as a shield to inhibit viral infections: SARS-CoV-2 as a model case study, J. Mater. Chem. B. 9 (2021) 4620–4642.
[48] A. Talan, A. Mishra, S.A. Eremin, J. Narang, A. Kumar, S. Gandhi, Ultrasensitive electrochemical immuno-sensing platform based on gold nanoparticles triggering chlorpyrifos detection in fruits and vegetables, Biosens. Bioelectron. 105 (2018) 14–21.
[49] J. Turkevich, P.C. Stevenson, J. Hillier, A study of the nucleation and growth processes in the synthesis of colloidal gold, Discuss. Faraday Soc. 11 (1951) 55–75.
[50] G. Frens, Controlled nucleation for the regulation of the particle size in monodisperse gold suspensions, Nat. Phys. Sci. (Lond.) 241 (1973) 20–22.
[51] D. Shahdeo, V. Kesarwani, D. Suhag, J. Ahmed, S.M. Alshehri, S. Gandhi, Self-assembled chitosan polymer intercalating peptide functionalized gold nanoparticles as nanoprobe for efficient imaging of urokinase plasminogen activator receptor in cancer diagnostics, Carbohydr. Polym. 266 (2021) 118138.
[52] S. Islam, Moinuddin, A.R. Mir, A. Raghav, S. Habib, K. Alam, A. Ali, Glycation, oxidation and glycoxidation of IgG: a biophysical, biochemical, immunological and hematological study, J. Biomol. Struct. Dyn. 36 (2018) 2637–2653.
[53] P. Zhou, X. Lou Yang, X.G. Wang, B. Hu, L. Zhang, W. Zhang, H.R. Si, Y. Zhu, B. Li,

C.L. Huang, H.D. Chen, J. Chen, Y. Luo, H. Guo, R. Di Jiang, M.Q. Liu, Y. Chen, X.R. Shen, X. Wang, X.S. Zheng, K. Zhao, Q.J. Chen, F. Deng, L.L. Liu, B. Yan, F.X. Zhan, Y.Y. Wang, G.F. Xiao, Z.L. Shi, A pneumonia outbreak associated with a new coronavirus of probable bat origin, Nature 579 (2020) 270–273.

[54] Y. Pan, H. Guan, S. Zhou, Y. Wang, Q. Li, T. Zhu, Q. Hu, L. Xia, Initial CT findings and temporal changes in patients with the novel coronavirus pneumonia (2019-nCoV): a study of 63 patients in Wuhan, China, Eur. Radiol. 30 (2020) 3306–3309.

[55] C. Ihling, D. Tänzler, S. Hagemann, A. Kehlen, S. Hüttelmaier, C. Arlt, A. Sinz, Mass spectrometric identification of SARS-CoV-2 proteins from gargle solution samples of COVID-19 patients, J. Proteome Res. 19 (2020) 4389–4392.

[56] C. Lucia, P.-B. Federico, G.C. Alejandra, An ultrasensitive, rapid, and portable coronavirus SARS-CoV-2 sequence detection 3 method based on CRISPR-Cas12, BioRxiv (2020) 1–10, https://doi.org/10.1101/2020.02.29.971127.

[57] J.P. Broughton, X. Deng, G. Yu, C.L. Fasching, V. Servellita, J. Singh, X. Miao, J.A. Streithorst, A. Granados, A. Sotomayor-Gonzalez, K. Zorn, A. Gopez, E. Hsu, W. Gu, S. Miller, C.Y. Pan, H. Guevara, D.A. Wadford, J.S. Chen, C.Y. Chiu, CRISPR–Cas12-based detection of SARS-CoV-2, Nat. Biotechnol. 38 (2020) 870–874.

[58] Z. Huang, D. Tian, Y. Liu, Z. Lin, C.J. Lyon, W. Lai, D. Fusco, A. Drouin, X. Yin, T. Hu, B. Ning, Ultra-sensitive and high-throughput CRISPR-p owered COVID-19 diagnosis, Biosens. Bioelectron. 164 (2020), 112316.

[59] M. El-Tholoth, H.H. Bau, J. Song, A single and two-stage, closed-tube, molecular test for the 2019 novel coronavirus (COVID-19) at home, clinic, and points of entry, Anal. Chem. 93 (2021) 13063–13071.

[60] W.E. Huang, B. Lim, C.C. Hsu, D. Xiong, W. Wu, Y. Yu, H. Jia, Y. Wang, Y. Zeng, M. Ji, H. Chang, X. Zhang, H. Wang, Z. Cui, RT-LAMP for rapid diagnosis of coronavirus SARS-CoV-2, Microb. Biotechnol. 13 (2020) 950–961.

[61] Y.H. Baek, J. Um, K.J.C. Antigua, J.H. Park, Y. Kim, S. Oh, Y. il Kim, W.S. Choi, S.G. Kim, J.H. Jeong, B.S. Chin, H.D.G. Nicolas, J.Y. Ahn, K.S. Shin, Y.K. Choi, J.S. Park, M.S. Song, Development of a reverse transcription-loop-mediated isothermal amplification as a rapid early-detection method for novel SARS-CoV-2, Emerg. Microb. Infect. 9 (2020) 998–1007.

[62] M.A. Lalli, S.J. Langmade, X Chen, C.C. Fronick, C.S. Sawyer, L.C. Burcea, M.N. Wilkinson, R.s. Fulton, M. Heinz, W.J. Buchser, R.D. Mitra, R.D. Head, R.D. Mitra, J. Milbrandt, Rapid and Extraction-Free Detection of SARS-CoV-2 from Saliva by Colorimetric Reverse-Transcription Loop-Mediated Isothermal Amplification, Clin. Chem . 67 (2021) 415–424.

[63] G. Qiu, Z. Gai, Y. Tao, J. Schmitt, G.A. Kullak-Ublick, J. Wang, Dual-functional plasmonic photothermal biosensors for highly accurate severe acute respiratory syndrome coronavirus 2 detection, ACS Nano 14 (2020) 5268–5277.

[64] A. Djaileb, B. Charron, M.H. Jodaylami, V. Thibault, J. Coutu, K. Stevenson, S. Forest, L.S. Live, D. Boudreau, J.N. Pelletier, J.-F. Masson, A rapid and quantitative serum test for SARS-CoV-2 antibodies with portable surface plasmon resonance sensing, ChemRxiv (2020), https://doi.org/10.26434/chemrxiv.12118914.v1.

[65] P. Moitra, M. Alafeef, M. Alafeef, M. Alafeef, K. Dighe, M.B. Frieman, D. Pan, D. Pan, D. Pan, Selective naked-eye detection of SARS-CoV-2 mediated by N gene targeted antisense oligonucleotide capped plasmonic nanoparticles, ACS Nano 14 (2020) 7617–7627.